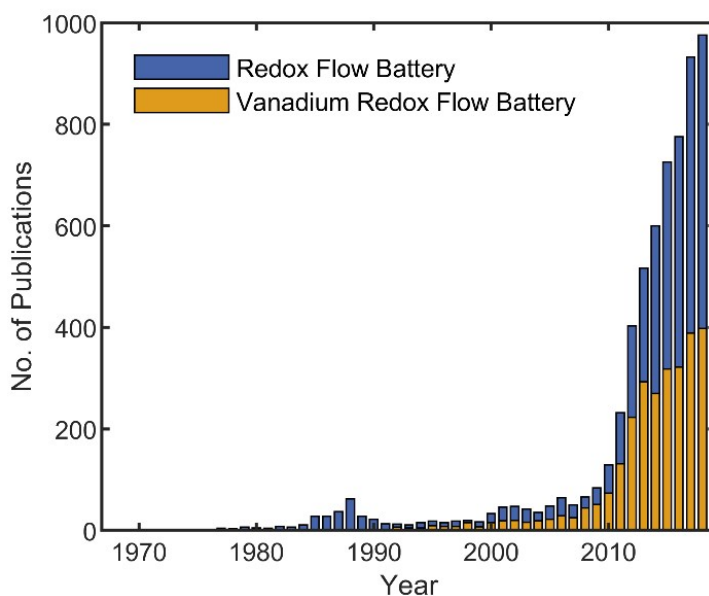


## Supporting Information

### Origin of the catalytic activity at graphite electrodes in vanadium flow batteries

Hannes Radinger, Ahmad Ghamlouche, Helmut Ehrenberg, Frieder Scheiba

*Institute for Applied Materials, Karlsruhe Institute of Technology, Hermann-von-Helmholtz-Platz  
1, 76344 Eggenstein-Leopoldshafen, Germany*



**Figure S1.** Number of publications in the flow battery field over the last 40 years. The results are based on a SciFinder analysis, in which the key words „redox flow battery“ and „vanadium redox flow battery“ are entered.

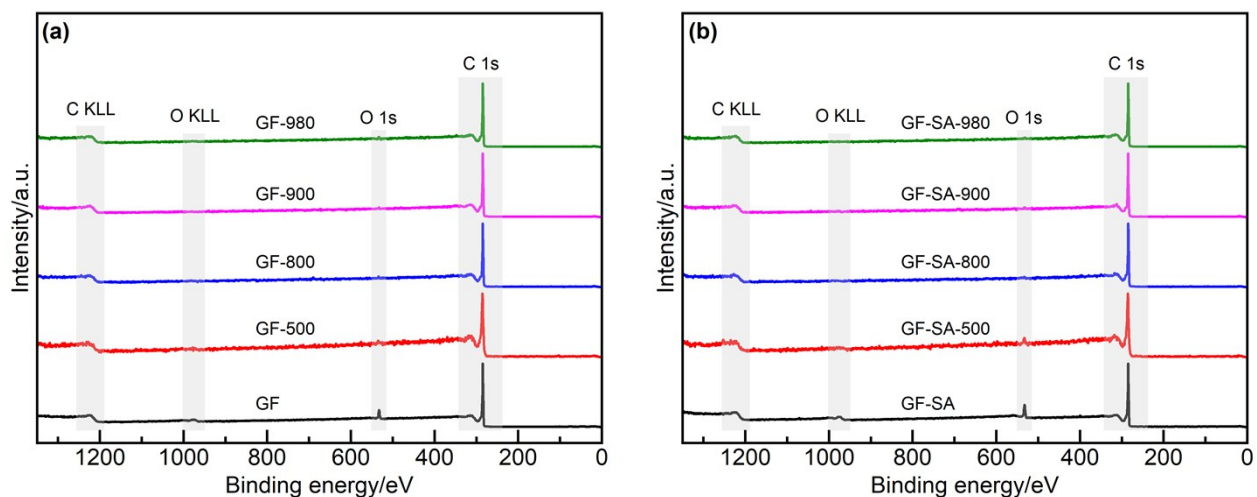


**Figure S2.** X-Ray photoelectron survey spectra recorded prior to the detailed XPS investigation. The spectra are given regarding the previous temperature treatment for (a) GF and (b) surface activated GF-SA. Only carbon and oxygen were detected as chemical compounds, as it is deduced from the carbon Auger C KLL ( $\sim 1223$  eV) and core level region C 1s ( $\sim 285$  eV), and equally from the oxygen Auger O KLL (1013-978 eV) and core level O 1s ( $\sim 531$  eV).<sup>1</sup> The degree of deoxygenation can already be observed in the surveys, as the contribution from the O 1s and the O KLL signals vanish after the temperature treatment.

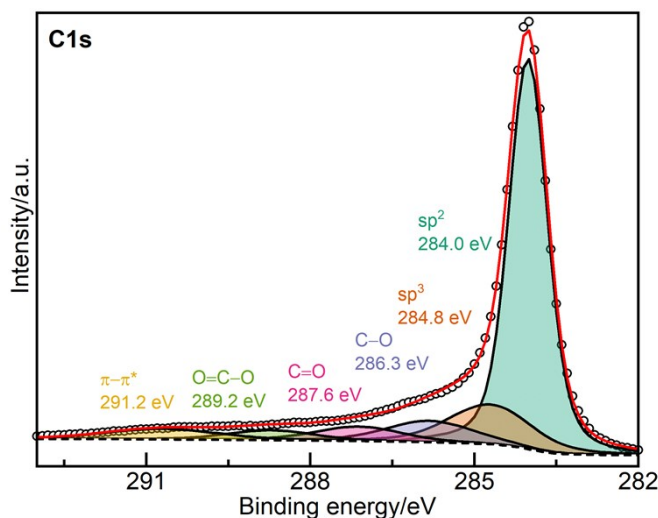


**Figure S3.** X-Ray photoelectron detail spectrum of the core-level C 1s of pristine graphite felt. Six different carbon related peak components are deconvoluted and indicated in the picture. The spectrum is binding energy corrected to the  $sp^2$  carbon component.  $sp^2$  hybridized carbon at 284 eV,  $sp^3$  carbon at 284.8 eV, ether and hydroxyl groups at 286.3 eV, carbonyls at 287.6 eV, and carboxylic groups at 289.2 eV; the additional  $sp^2$  carbon related shake-up satellite is located at 291.2 eV.<sup>2-5</sup>

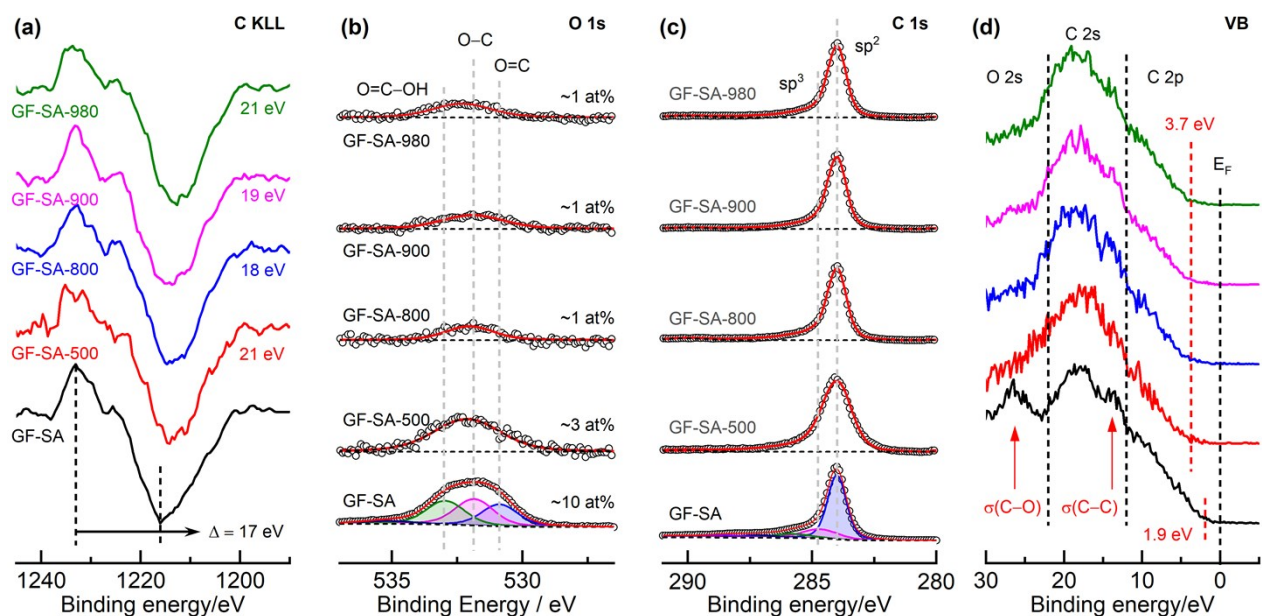


**Figure S4.** X-Ray photoelectron spectroscopy investigation of the electronic structure of thermally deoxygenated, previously surface-activated graphite felts. (a) First derivative of the C KLL Auger region to determine the D-parameter. (b) O 1s detail spectra, indicating the position of the respective oxygen group and the relative oxygen content. (c) C 1s detail spectra, indicating the position of sp<sup>2</sup> and sp<sup>3</sup> hybridized carbon. (d) Valence band region, displaying the O 2s, C 2s and C 2p regions and the evaluated valence band maximum.

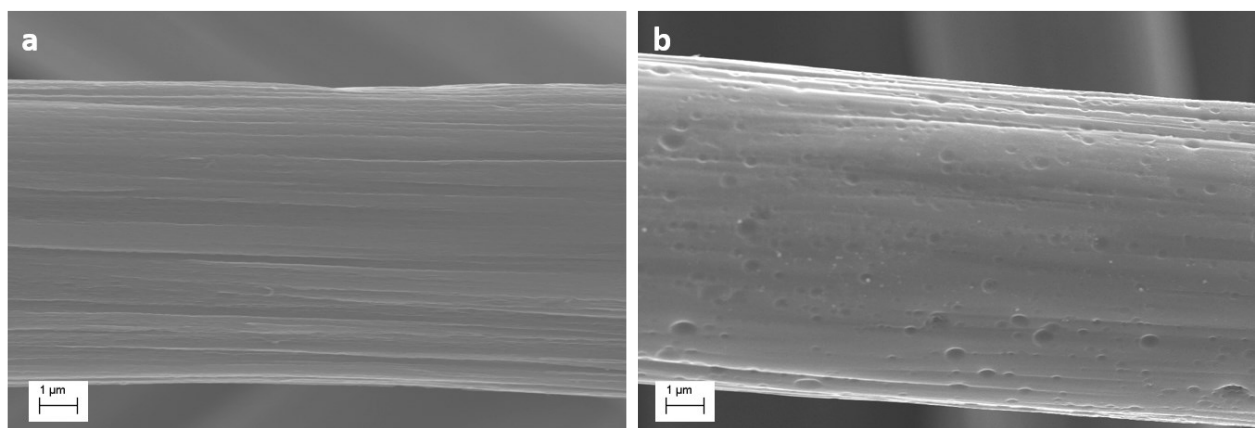


**Figure S5.** Scanning electron microscopy of thermally deoxygenated GF-980 and GF-SA-980.

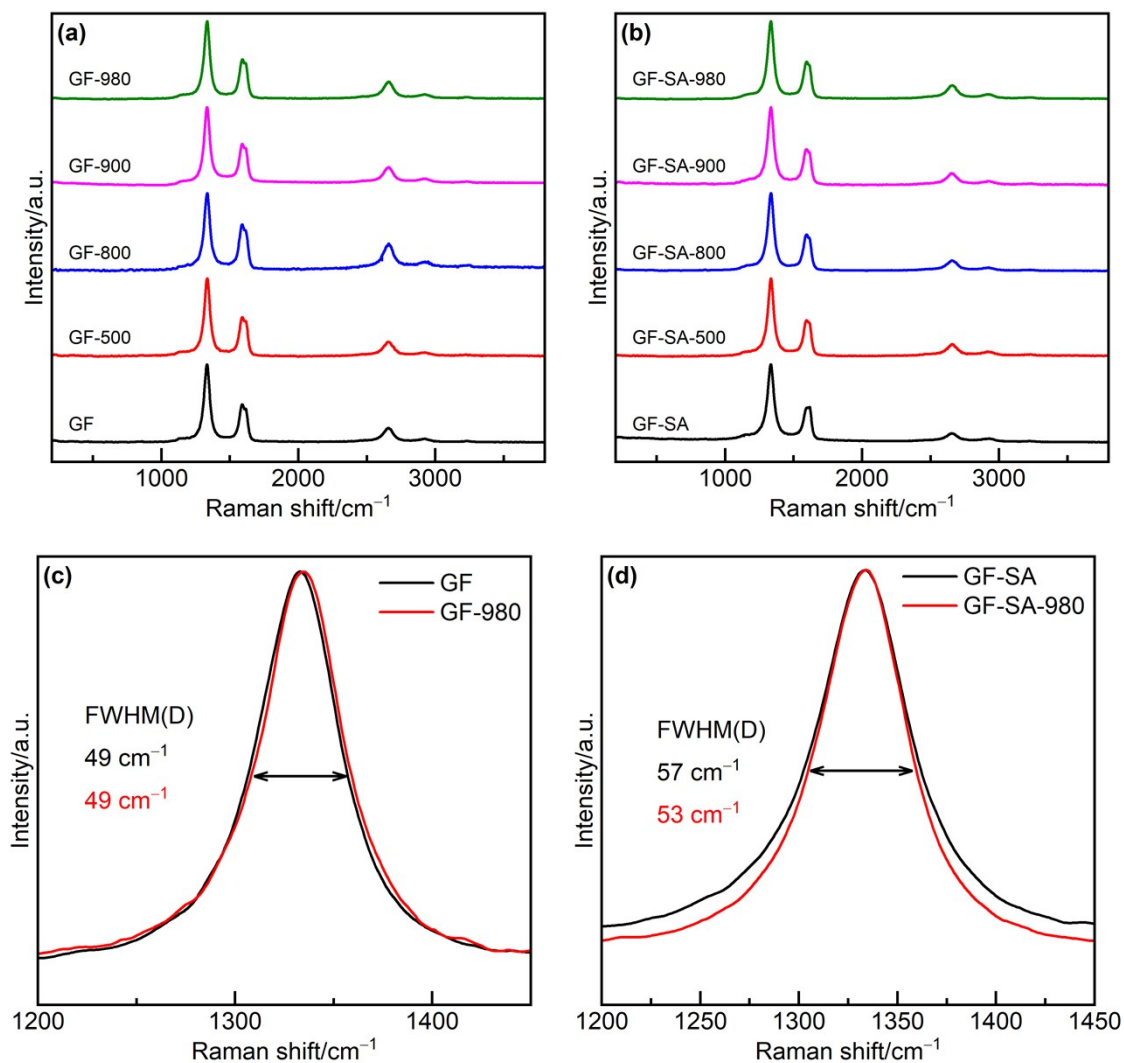


**Figure S6.** Raman spectra of (a) pristine and (b) surface-activated graphite felts prior to and after each corresponding deoxygenation step. The spectra in the picture are normalized to the D band, but not background corrected or deconvoluted. For the assessment of the singular signals of the D, G, and D' bands, the spectra have been subtracted by a cubic spline and fitted with Gaussian-Lorentzian peak shapes. Details to this procedure are given in the Experimental Section. (c,d) depiction of the D band of pristine and fully deoxygenated GF and GF-SA electrodes to evaluate the FWHM.

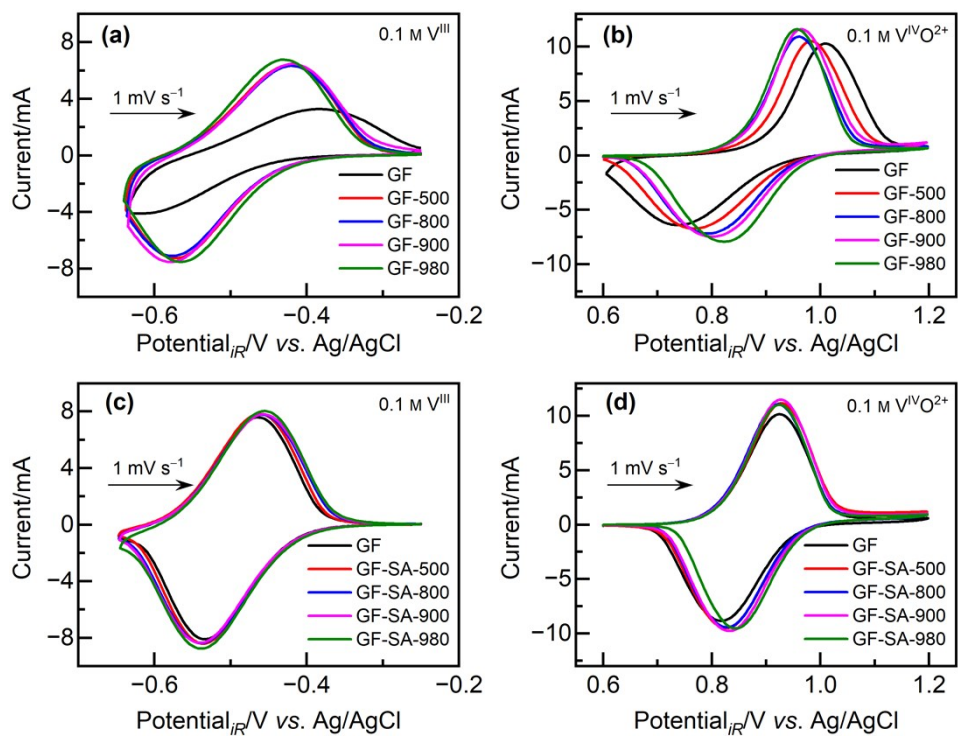


**Figure S7.** Electrochemical activity towards the  $V^{III}/V^{II}$  (*i.e.* the negative half-cell reaction in a VFRB) and the  $V^{VO_2^+}/V^{IVO_2^+}$  (*i.e.* the positive half-cell reaction) studied by cyclic voltammetry in a three-electrode cell. As electrolyte, 0.1 M  $V^{III}$  and  $V^{IVO_2^+}$  in 2 M  $H_2SO_4$  has been used. Voltammograms were recorded with a scan rate of  $1 \text{ mV s}^{-1}$ . (a–b) CV data for pristine and deoxygenated GF; (c–d) for thermally surface activated and deoxygenated GF-SA.

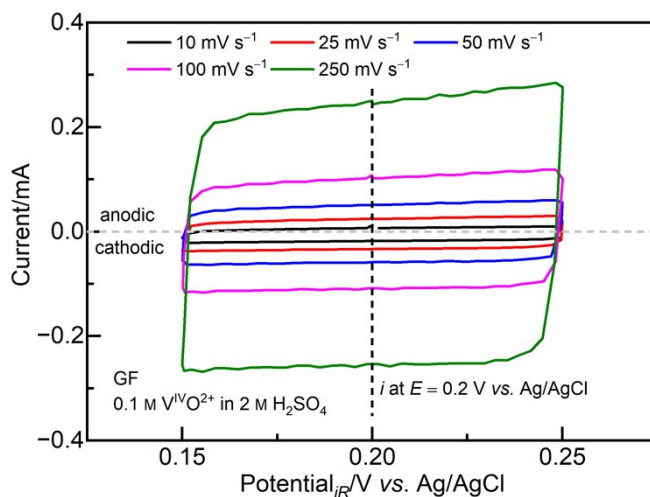


**Figure S8.** Example of the used CV method to evaluate the electrical double layer capacitance. CV is recorded in the positive electrolyte in a non-faradaic potential region with varying scan rates. Afterwards, the current at the (arbitrary) potential of 0.2 V vs. Ag/AgCl is used and plotted against the scan rate (see Figure 4d).

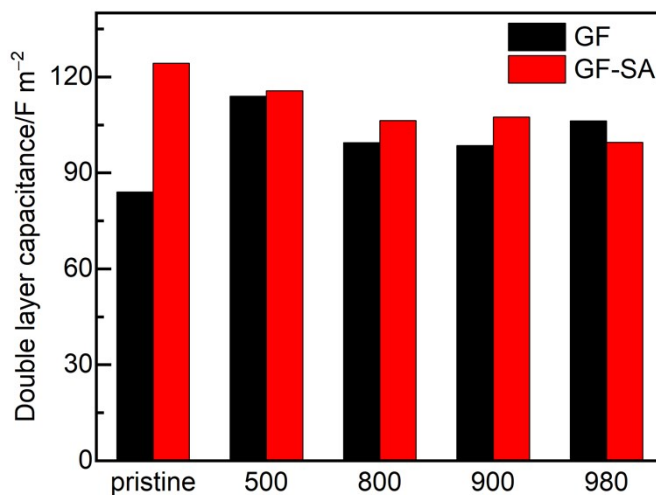


**Figure S9.** Normalized electrical double layer capacitance (EDLC) of graphite felt electrodes. The EDLC has been evaluated by a CV method described in the Experimental Section. The surface area of the felt was measured by BET; the weight of the electrode was determined prior to electrochemical cycling.

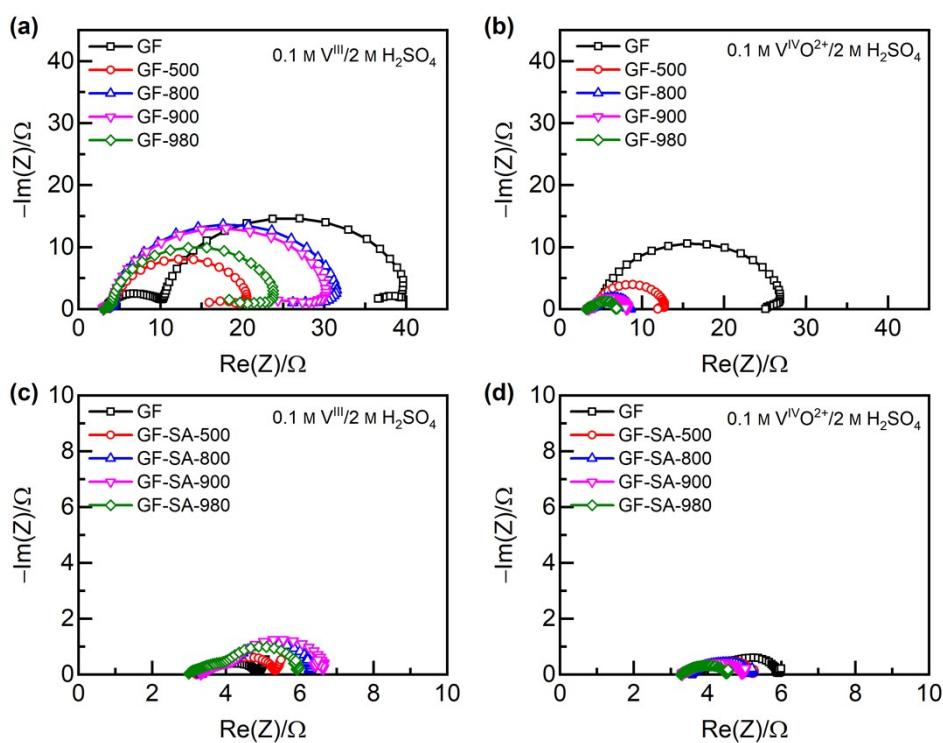


**Figure S10.** Nyquist plots of electrochemical impedance measurements. Displayed are the negative and positive half-cell measurements at an applied potential of  $-0.45$  and  $0.9$  V vs.

Ag/AgCl for pristine and at various temperatures thermally deoxygenated (a–b) GF and (c–d) GF-SA.

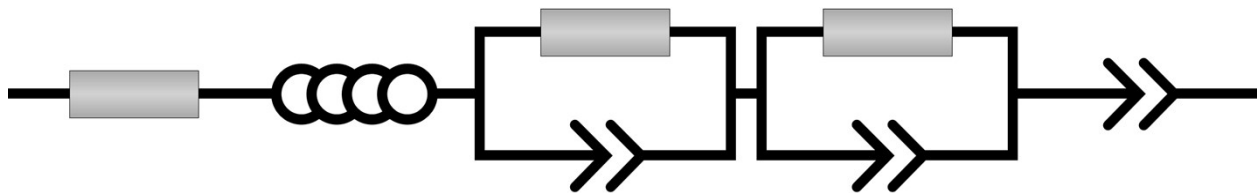


**Figure S11.** Equivalent Circuit diagram that has been used for the fitting procedure of the EIS data. The graph displays following elements: an inductance and the electrolyte resistance in series, followed by two resistance/constant phase elements in parallel, one for the glassy carbon/felt, and one for the felt/electrolyte interface, and in the end one constant phase element for the diffusion. Herein we note, that not for every spectrum every element was necessary, which applies to the inductance and the last constant phase element. The value for the electrolyte resistance was used to correct the CV diagrams, the resistance value of the felt/electrolyte interface is determined as the charge-transfer resistance.

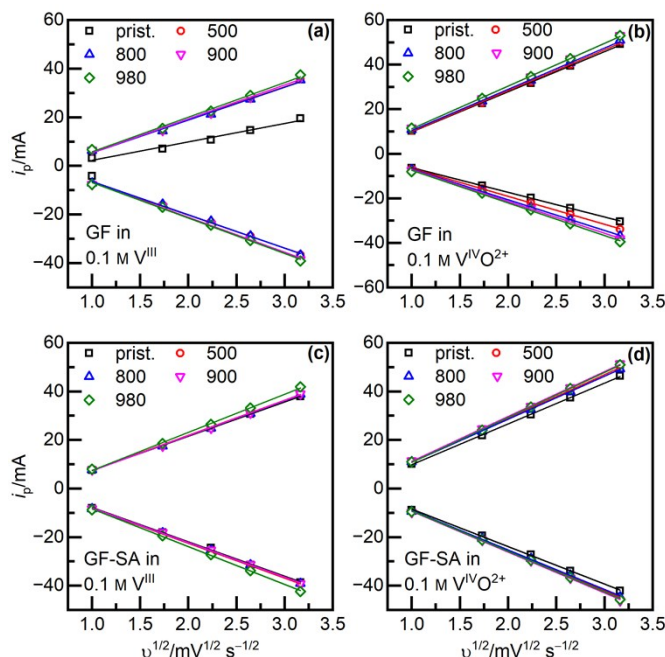


**Figure S12.** Randles-Sevcik plots of pristine and deoxygenated felt electrodes in both half-cells. As electrolyte, 0.1 M  $V^{III}$  and  $V^{IV}O^{2+}$  in 2 M  $H_2SO_4$  has been used. (a–b) CV data for pristine and deoxygenated GF; (c–d) for thermally surface activated and deoxygenated GF-SA. The data has been determined from the peak currents of CV scans with varying scan rates. The linearity of  $v^{1/2}$

vs. the peak currents  $i_p$  suggests a chemically reversible redox process limited by diffusion, whereas an increased slope is characteristic for a fast mass transfer.<sup>6,7</sup>

**Note to Figure S12:**

Mass transfer properties have been investigated by graphically verifying the Randles–Sevcik equation, which shows a linearity of  $i_p$  vs.  $\nu^{1/2}$  for all electrodes in both half-cells, indicating a chemically reversible redox process limited by diffusion.<sup>6,8,9</sup> A higher slope therein suggests a faster mass transfer process, which has been observed especially for the  $V^{III}/V^{II}$  redox reaction after heat treatment.<sup>7</sup> The most rapid mass transfer is always achieved for felts deoxygenated at 980 °C, which is another indicator for the hindering effect of OFGs. Since the vanadium (oxide) species must move towards the active edge sites of the felt, the diffusional properties along an oxygen-free basal plane are important. The thermal deoxygenation treatment further creates additional active sites on GF that as well contribute to the higher  $i_p$  values observed.

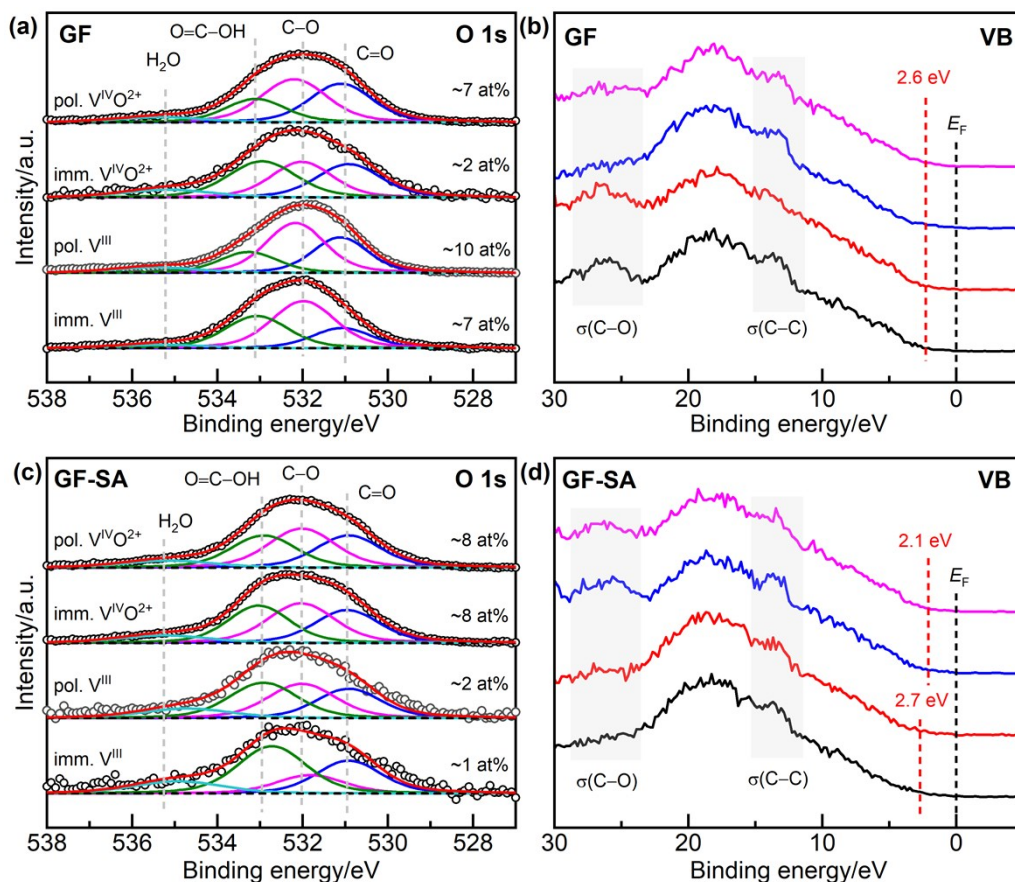


**Figure S13.** X-Ray photoelectron spectroscopy investigation of the electronic structure of previously thermally deoxygenated pristine and surface activated graphite felts. The felt electrodes have either been immersed in vanadium electrolyte for 3 h or have been polarized at an applied potential of  $-0.6$  and  $1.2$  V vs. Ag/AgCl in V<sup>III</sup> and V<sup>IV</sup>O<sub>2</sub><sup>+</sup> for 1h, respectively. The figure displays the O 1s detail spectra and the valence band region of (a–b) GF and (c–d) GF-SA, each after deoxygenation at  $980$  °C and respective electrolyte treatment.

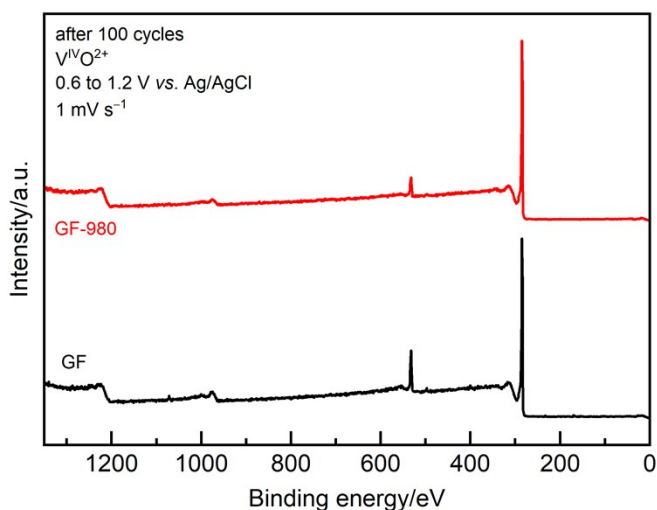


**Figure S14.** X-Ray photoelectron survey spectra of 100 times cycled pristine (GF) and deoxygenated (GF-980) graphite felt. Only carbon and oxygen were detected as chemical compounds, as it is deduced from the carbon Auger C KLL ( $\sim 1223$  eV) and core level region C 1s ( $\sim 285$  eV), and equally from the oxygen Auger O KLL (1013-978 eV) and core level O 1s ( $\sim 531$  eV).<sup>1</sup>

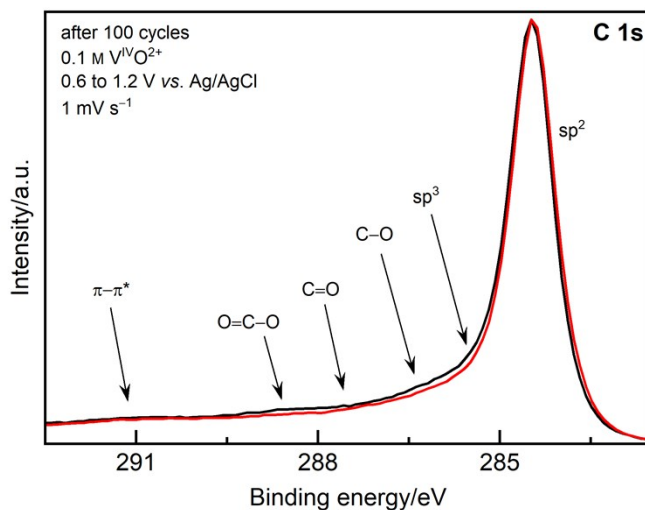


**Figure S15.** Normalized C 1s detail spectra with the estimated positions of the single compounds indicated. Due to its complexity, the C 1s detail region is not used for a quantitative fitting approach, but a direct comparison of the normalized detail spectra yields a qualitative difference of the samples in an increased  $sp^3$  carbon signal and various carbon-oxygen bonding signals that are more pronounced for GF.

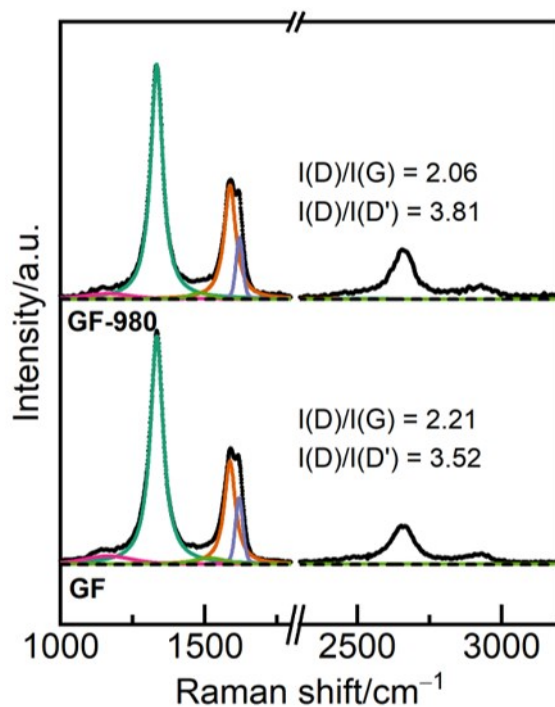


**Figure S16.** Deconvoluted Raman spectra to evaluate the degree of disorder after long-term cycling. The band intensity ratios are indicated for each sample. While the  $I(D)/I(D')$  ratio stays the same compared to the electrode before cycling, the  $I(D)/I(G)$  ratio changes substantially.

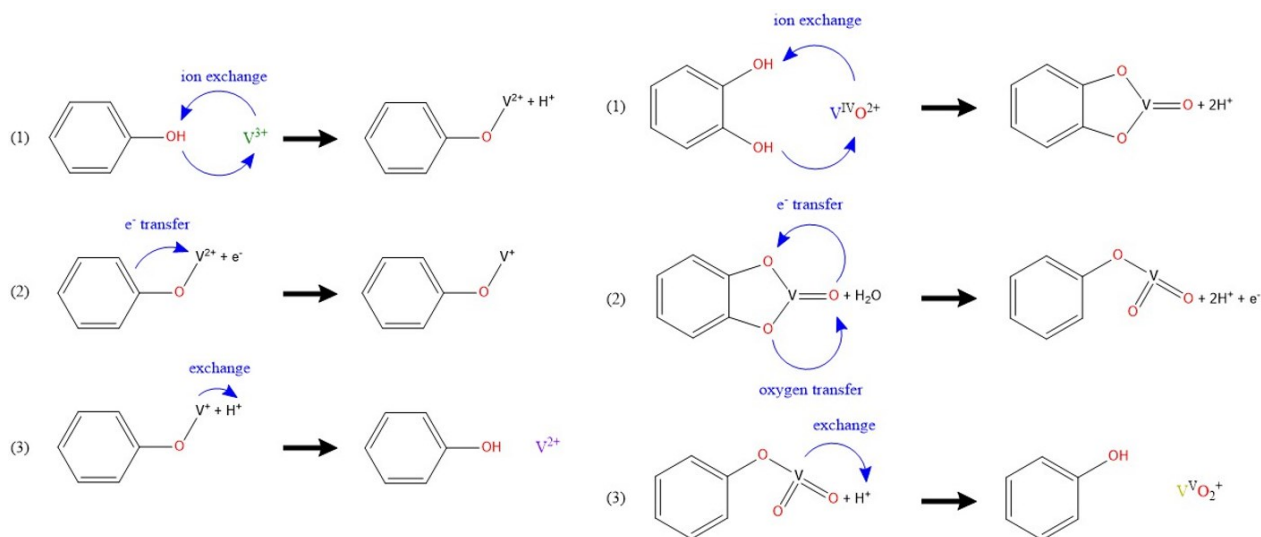


**Figure S17.** Old reaction mechanism via hydroxyl groups, first proposed in 1992.<sup>10</sup> The left panel displays the mechanism in the negative half-cell *via* an ion exchange mechanism, followed by the electron transfer and another ion exchange mechanism. The left panel shows the mechanism in the positive half-cell in a similar order, but with two initial hydroxyl groups at the electrode surface.

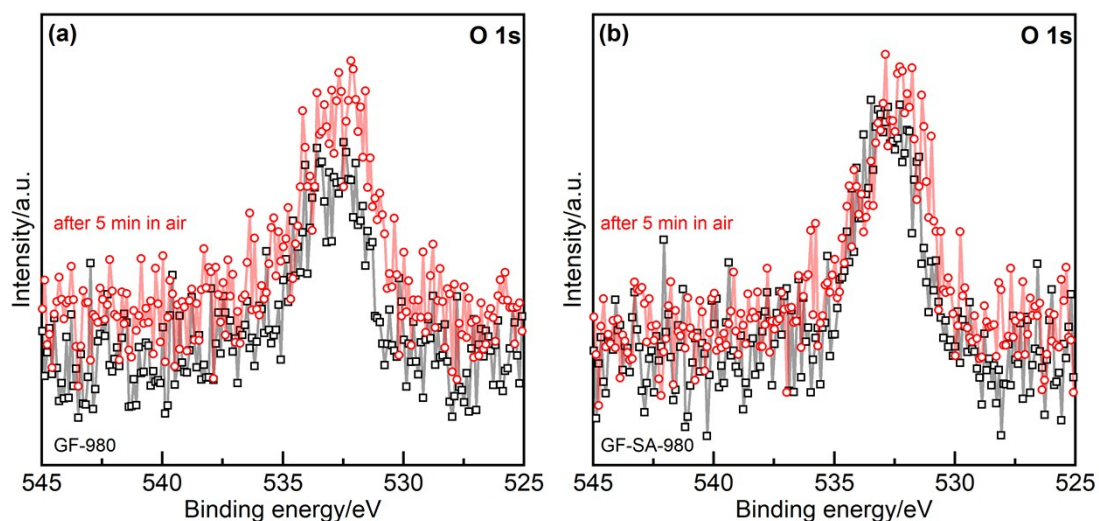


**Figure S18.** X-Ray photoelectron spectroscopy investigation to examine the self-oxidation of deoxygenated graphite felt in contact with atmosphere. The previously measured felts were exposed to atmosphere for 5 min in the load lock of the XPS chamber. Afterwards, spectra were recorded again at the same spot. The figure displays the deoxygenated pristine (a) and surface-activated (b) felt electrode.

## References

1. Moulder, J. F. & Chastain, J. (eds.). *Handbook of X-ray photoelectron spectroscopy. A reference book of standard spectra for identification and interpretation of XPS data* (Perkin-Elmer Corporation, Eden Prairie, Minn., 1992).
2. Ganguly, A., Sharma, S., Papakonstantinou, P. & Hamilton, J. Probing the Thermal Deoxygenation of Graphene Oxide Using High-Resolution In Situ X-ray-Based Spectroscopies. *J. Phys. Chem. C* **115**, 17009–17019; 10.1021/jp203741y (2011).
3. Chen, L. *et al.* Modifying graphite oxide nanostructures in various media by high-energy irradiation. *RSC Adv* **4**, 1025–1031; 10.1039/C3RA46203J (2014).
4. Park, S. *et al.* Graphene oxide papers modified by divalent ions-enhancing mechanical properties via chemical cross-linking. *ACS nano* **2**, 572–578; 10.1021/nn700349a (2008).
5. Estevez, L. *et al.* Tunable Oxygen Functional Groups as Electrocatalysts on Graphite Felt Surfaces for All-Vanadium Flow Batteries. *ChemSusChem* **9**, 1455–1461; 10.1002/cssc.201600198 (2016).
6. Li, W. *et al.* Graphene-Nanowall-Decorated Carbon Felt with Excellent Electrochemical Activity Toward  $\text{VO}_2^+/\text{VO}_2$  Couple for All Vanadium Redox Flow Battery. *Advanced science (Weinheim, Baden-Württemberg, Germany)* **3**, 1500276; 10.1002/advs.201500276 (2016).

7. Park, M., Ryu, J., Kim, Y. & Cho, J. Corn protein-derived nitrogen-doped carbon materials with oxygen-rich functional groups: a highly efficient electrocatalyst for all-vanadium redox flow batteries. *Energy Environ. Sci.* **7**, 3727–3735; 10.1039/C4EE02123A (2014).
8. Huang, R.-H. *et al.* Investigation of Active Electrodes Modified with Platinum/Multiwalled Carbon Nanotube for Vanadium Redox Flow Battery. *J. Electrochem. Soc.* **159**, A1579-A1586; 10.1149/2.003210jes (2012).
9. Han, P. *et al.* Graphene oxide nanoplatelets as excellent electrochemical active materials for VO<sub>2</sub><sup>+/0</sup> and V<sup>2+</sup>/V<sup>3+</sup> redox couples for a vanadium redox flow battery. *Carbon* **49**, 693–700; 10.1016/j.carbon.2010.10.022 (2011).
10. Sun, B. & Skyllas-Kazacos, M. Modification of graphite electrode materials for vanadium redox flow battery application—I. Thermal treatment. *Electrochimica Acta* **37**, 1253–1260; 10.1016/0013-4686(92)85064-R (1992).